Subduction erosion and basal friction along the sediment-starved convergent margin off Antofagasta, Chile

R. von Huene and C. R. Ranero

GEOMAR, Research Center for Marine Geosciences, Christian Albrechts University, Kiel, Germany

Received 12 October 2001; revised 3 March 2002; accepted 7 May 2002; published 6 February 2003.

[1] Subduction erosion is commonly associated with strong interplate coupling and a consequent abrasion of the upper plate. Northern Chile is an often cited example of a strongly coupled erosional margin. Its crystalline basement is inferred to form a strong upper plate, the trench axis contains little detectable sediment, and the subducting lower plate has a high-relief horst-graben topography. With little water-rich sediment to reduce interplate friction, the high relief of an igneous ocean crust thrust beneath continental basement should generate high friction interplate abrasion. However, a prestack depth-migrated seismic record images slope debris that collects in a frontal prism. This debris, including ~30% pore fluid, fills subducting grabens and is subsequently incorporated into an ~1.5-km-thick interplate reflective layer. The subduction zone thrust passes through the upper part of this layer. Interplate seismicity and taper analyses indicate basal friction at levels that are common in sedimented convergent margins. The continued growth of lower plate grabens after subduction probably accommodates upper plate material, a process that erodes the upper plate. Erosion is aided by weakening of the upper plate rock framework beneath the continental slope. This erosion undermines the upper plate and tips it seaward thereby steepening the continental slope which induces midslope gravity tectonics. Despite sediment starvation, a frontal prism constructed of remolded slope debris elevates pore pressure to reduce interplate friction. Coeval erosion and prism building control the size of the frontal prism. Processes other than high friction abrasion best explain subduction erosion along northern Chile. *INDEX TERMS:* 3045 Marine Geology and Geophysics: Seafloor morphology and bottom photography; 0935 Exploration Geophysics: Seismic methods (3025); 3040 Marine Geology and Geophysics: Plate tectonics (8150, 8155, 8157, 8158); 9360 Information Related to Geographic Region: South America; *KEYWORDS:* convergent margin, tectonic processes, subduction erosion

Citation: von Huene, R., and C. R. Ranero, Subduction erosion and basal friction along the sediment-starved convergent margin off Antofagasta, Chile, *J. Geophys. Res.*, *108*(B2), 2079, doi:10.1029/2001JB001569, 2003.

1. Introduction

[2] Subduction erosion has affected most of the world's convergent margins but the mechanisms that erode are much less understood than those that accrete ocean sediment at subduction zones. In cartoons, erosion is commonly depicted as a vertically exaggerated horst and graben subducting plate morphology that abrades the underside of the upper plate under conditions of high friction. Such abrasion is not imaged in seismic records and horst and graben seafloor roughness is commonly overwhelmed by sediment which smoothes lower plate relief immediately before subduction [cf. *McCarthy and Scholl*, 1985].

[3] Many investigators accepted the idea of tectonic erosion along the underside of the upper plate from abrasive scraping by subducting horst and graben relief on the lower plate [*Hilde*, 1983]. Presumably this requires high friction and high compressional stress [*Jarrard*, 1986]. Puzzling then is the pervasive extensional tectonism of the northern Chile coastal and offshore area. Extension across the Mejillones Peninsula is explained by uplift from underplated material and stretching of the overlying crust [i.e., *Delouis et al.*, 1998].

[4] Convergent margins are both sediment dominated and sediment starved. The northern Chile margin is an example of a sediment-starved margin because here continental basement forms the upper plate, the ocean crust is thinly sedimented, and the trench axis is virtually empty of a turbidite sequence [*Scholl et al.*, 1970; *Kulm et al.*, 1977; *Hinz et al.,* 1998]. More than 30 years ago it was recognized by some that the tectonics of this margin is dominated by subduction erosion [*Miller*, 1970; *Rutland*, 1971]. The issue addressed here is whether this zone of convergence with little water-rich sediment to reduce interplate friction is in fact highly abrasive and thus prone to subduction erosion or whether strong coupling beneath continental slope is involved at all. We wondered if seismic data across such a margin would reveal structure associated with subduction erosion despite lack of reflective sediment strata to define

0148-0227/03/2001JB001569$09.00

deformation and subducted relief. A seismic reflection line off the Mejillones Peninsula just north of Antofagasta (23°S) acquired by the Bundesanstalt fuer Geowissenschaften und Rohstoffe (BGR, Hannover Germany) during the Crustal Investigations Off- and Onshore Nazca/Central Andes (CINCA) investigation [*Hinz et al.*, 1995] was released to us for prestack depth migration. The seismic line is complimented by extensive multibeam bathymetry [*von Huene et al.*, 1999], single-channel seismic reflection data [*Scholl et al.*, 1970], a refraction seismic transect [*Patzwald et al.*, 1999], and a seismogenic zone well located with records from a local seismometer network that recorded the 1995 Antofagasta earthquake (M_w = 8) aftershock sequence [*Husen et al.*, 2000; *Patzig*, 2000]. These observational data reveal conditions along an eroding plate boundary that indicate subduction erosion without involving strong coupling. The upper plate is dominated by extensional structure, and plate boundary conditions are similar to those recorded along sediment flooded margins. These observations and our explanations have general implications for processes that cause subduction erosion.

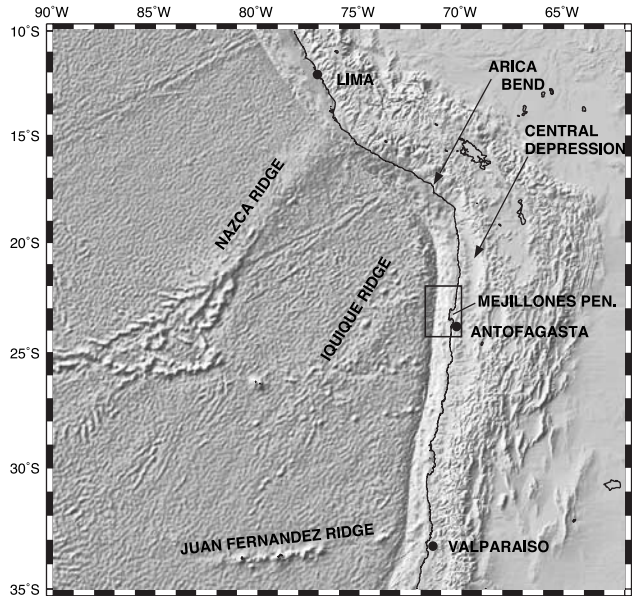

Figure 1. Location of the study area shown by rectangle on a satellite bathymetric and land topographic base.

2. Regional Setting and Previous Investigations

[5] Subduction erosion along northern Chile is indicated by outcrops of Mesozoic volcanic arcs in coastal cliffs and the landward migration of volcanic arcs during the past 100 Myr [cf. *Rutland*, 1971; *Scholl et al.*, 1980; *Armijo and Thiele*, 1990; *Delouis et al.*, 1998; *Hartley et al.*, 2000]. Even without clear marine seismic reflection images, it was argued that tectonic erosion had produced a continental slope of truncated continental basement. An arid climate and inland basins that trap erosional debris reduces the supply of sediment to the slope [*Hartley and Chong*, 2002] and to the trench axis as was inferred from early bathymetric profiles [i.e., *Fisher and Raitt*, 1962; *Hayes*, 1966]. A scarcity of slope or tectonically accreted ocean sediment became apparent in early seismic records and sparse gravity anomalies [*Fisher and Raitt*, 1962; *Scholl et al*, 1970; *Couch et al.*, 1981; *von Huene*, 1989]. A subduction zone without entrained sediment to reduce friction was anticipated by *Kulm et al.* [1977].

[6] South of the Arica bend, a near linear coastline characterizes the Chilean margin except at the Mejillones Peninsula just north of Antofagasta (Figure 1). A trench paralleling the coast [*Schweller and Kulm*, 1978] and marine gravity anomalies have the same remarkably linear trend [*Koesters et al.*, 1997]. However, Mejillones Peninsula protrudes seaward from this linear coast and is adjacent to the >8 km trench depth just 85 km seaward from the 1-km-high crest of the Peninsula, [*von Huene et al.*, 1999]. Presumably this great topographic relief is associated with subduction of the oldest ocean lithosphere along South America since old lithosphere is less buoyant than young lithosphere.

[7] Rock of the continental slope has a high acoustic velocity [*Fisher and Rait*, 1962; *Husen et al.*, 2000] and dredging offshore sampled formations that crop out on shore [*Rötzler et al.*, 1998]. Along northern Chile, the Coastal Cordillera consists predominantly of the 10-km-thick andesitic La Negra Formation of mid-Jurassic age and associated Mesozoic granitic intrusions [*Hartley et al.*, 1992]. The La Negra unconformably overlies Triassic and Paleozoic metamorphosed sedimentary rock and is overlain by Lower Cretaceous sedimentary rock. Resting unconformably on late Paleozoic and Mesozoic basement rocks are Miocene to Holocene marine and nonmarine sedimentary sequences.

[8] The basement unconformably overlain by mid-Miocene and younger marine sediment continues offshore as indicated by samples of Miocene age recovered during the Downwind Expedition [*Bandy and Rudolfo*, 1964]. During CINCA, 14 more sites with Miocene samples were dredged on the slope [*Kudrass et al.*, 1998]. In the coastal area of Mejillones Peninsula, Miocene sediment-filled shallow depressions and was overlapped by widespread early Pliocene sediment [*Hartley and Jolley*, 1995]. Pliocene uplift of the Peninsula resulted in elevated terraces, paleoseacliffs cut into the marine sediment and basement, and a series of paleoshorelines on the northern side of the peninsula [*Niemeyer et al.*, 1996].

[9] Neogene to Holocene vertical displacement formed large basins from the Coastal Cordillera to the pre-Andes. The Central Depression (Figure 1) collected thick sedimentary sequences during the past 20 Myr [*Hartley and Jolley*, 1995]. Sedimentation here and an arid climate since middle Miocene time reduced sediment transport across the rising Coastal Cordillera. The nearest Andean drainages crossing the cordillera and reaching the coast are 420 km north and 300 km south of the Mejillones Peninsula. Terrigeneous sediment perhaps 500 m thick was imaged seismically on the narrow shelf and upper slope [*Scholl et al.*, 1970; *Block*, 1998]. Significant here is the limited sediment transported from land during the past ~20 Myr, reduced northward axial transport down the trench axis caused by axial obstruction of the Juan Fernandez Ridge [*Yañez et al.*, 2001] (Figure 1), and the thin sediment layer carried on the ocean crust into the trench. No convergent continental margin adjacent to a high mountain range is more sediment starved than the northern Chile margin.

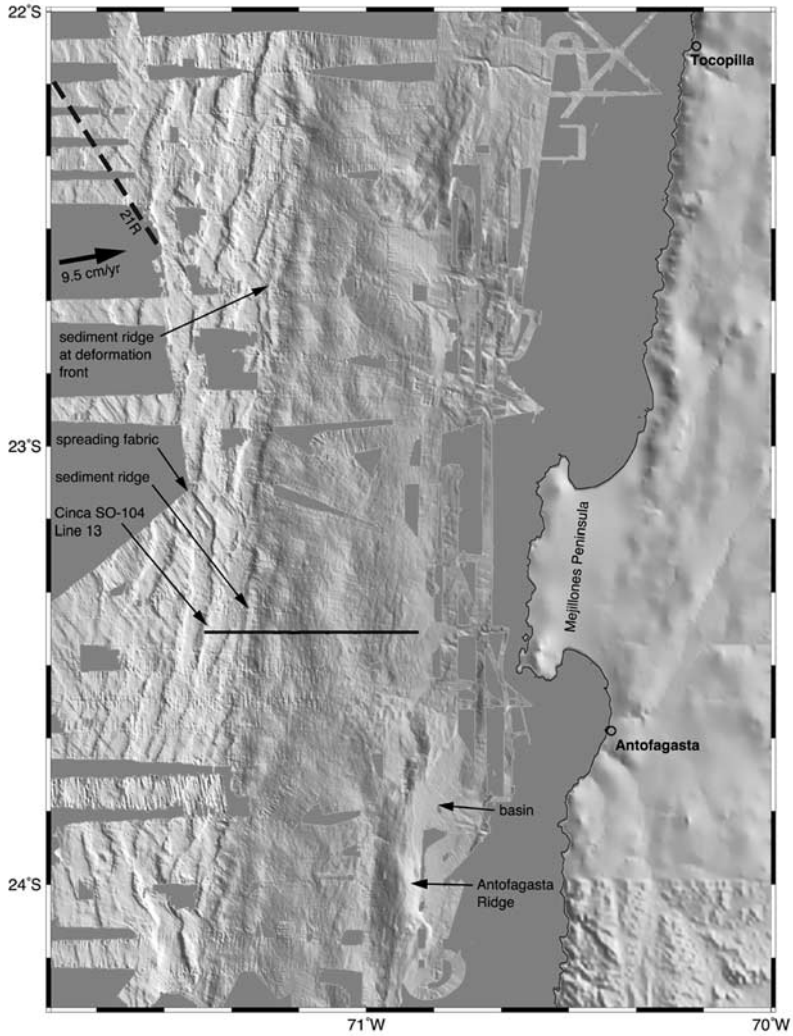

Figure 2. Shaded relief map of swath bathymetry with annotated features. Gray areas indicate no multibeam bathymetric data. CINCA SO104-13 is a multichannel seismic reflection line shown in Figure 5. Sediment ridge refers to slope detritus thrust faulted along the deformation front. See color version of this figure at back of this issue.

[10] Normal faults from the coast inland indicate east-west extension [cf. *Armijo and Thiele*, 1990; *Delouis et al.*, 1998; *Hartley et al.*, 2000]. Offshore, north trending extensional structures along the shelf edge and upper slope are imaged with multibeam bathymetry [*von Huene et al.*, 1999]. Gravity tectonics and mass wasting break down this morphology where the upper slope coalesces into a midslope. Midslope morphology is extensively smoothed by debris from coastal erosion and mass wasting (Figure 2). On the lower slope, the debris blanket drapes over subducting topography and is compressionally deformed. In the 2° long surveyed area, (Figures 2 and 3) one slope basin occurs off Antofagasta behind the prominent Antofagasta Ridge and similar basins are imaged to the south [*Scholl et al.*, 1970; *Block*, 1998].

[11] On the ocean floor, horst and graben faulting begins about 50–65 km seaward of the trench axis where the ocean crust begins to flex into the trench (Figure 4) [*Scholl et al.*, 1970; *Schweller and Kulm*, 1978; *Hinz et al.*, 1998]. Flexure reactivates structures formed at the spreading ridge that impart a pervasive crosscutting fabric in the morphology (Figure 2). Horsts and grabens between 22°S and 24°S locally have a relief up to 800 m but even near the trench axis where crustal flexure is greatest most of them do not exceed 500 m.

[12] A critical taper analysis as described by *Dahlen* [1984] and *Lallemand et al.* [1994] was applied to study mechanisms of subduction erosion in a transect across the margin including the Mejillones Peninsula by *Adam and Reuther* [2000]. They interpreted a slightly over-critical wedge as decreasing its taper by extending above an inferred midcrustal detachment and concluded that long-term erosion is a high basal friction process beneath the lower slope.

[13] The seismogenic zone is exceptionally well defined because the great M_w = 8.0 Antofagasta earthquake aftershock sequence occurred during deployment of marine and land instruments around Antofagasta. The 35 seismometers on land and 9 OBH instruments on the continental slope provided records that allowed precise location of the seismogenic zone and its updip and downdip limits [*Delouis et al.*, 1997; *Husen et al.*, 2000; *Patzig*, 2000]. Well-located

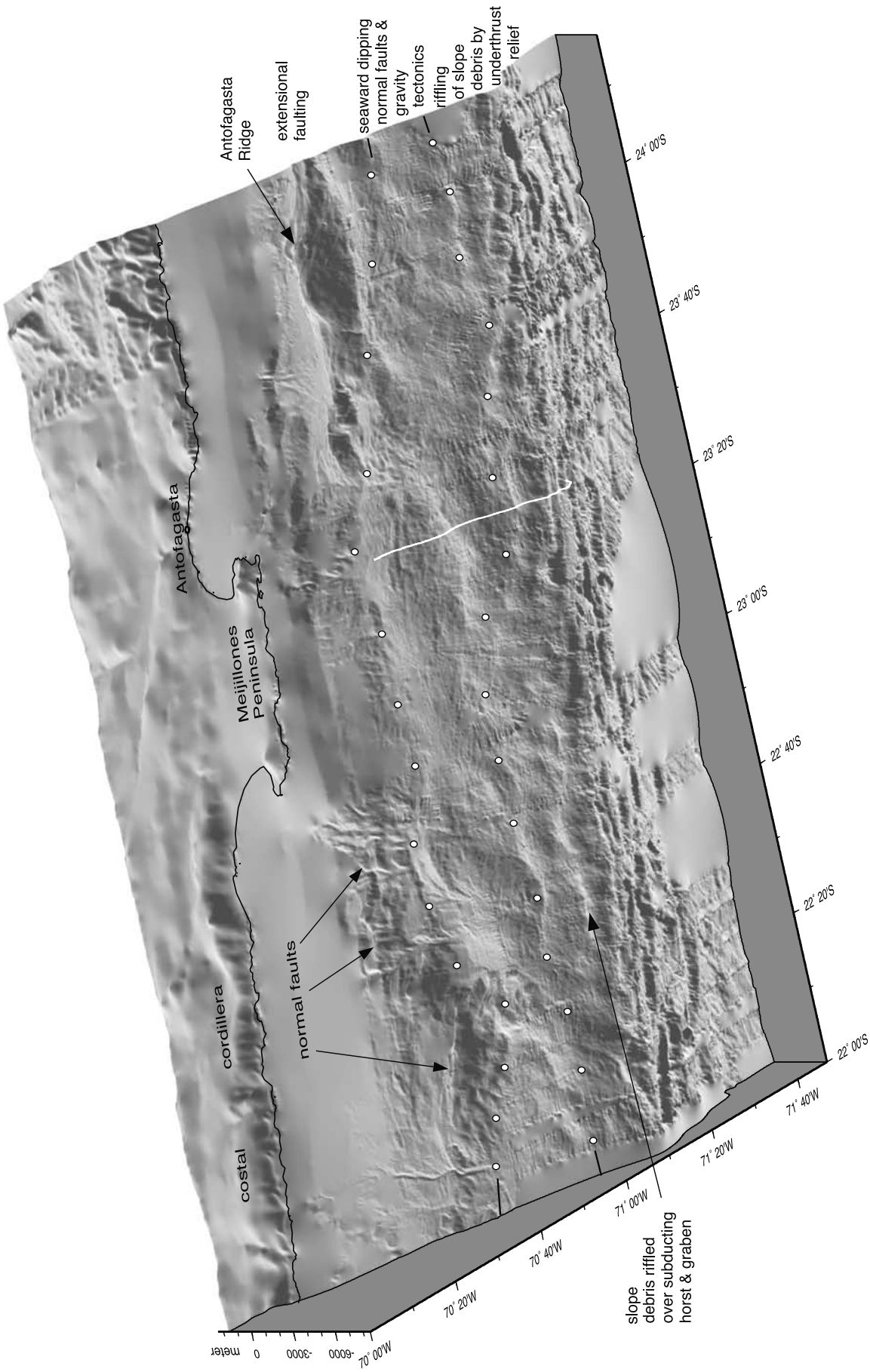

Figure 3a. Shaded relief perspective diagram. White line is seismic reflection line in Figure 5. Open circles separate morphotectonic zones interpreted in seismic sections. Note the similarity in size of Antofagasta Ridge and its sediment-ponded basin relative to Mejillones Peninsula.

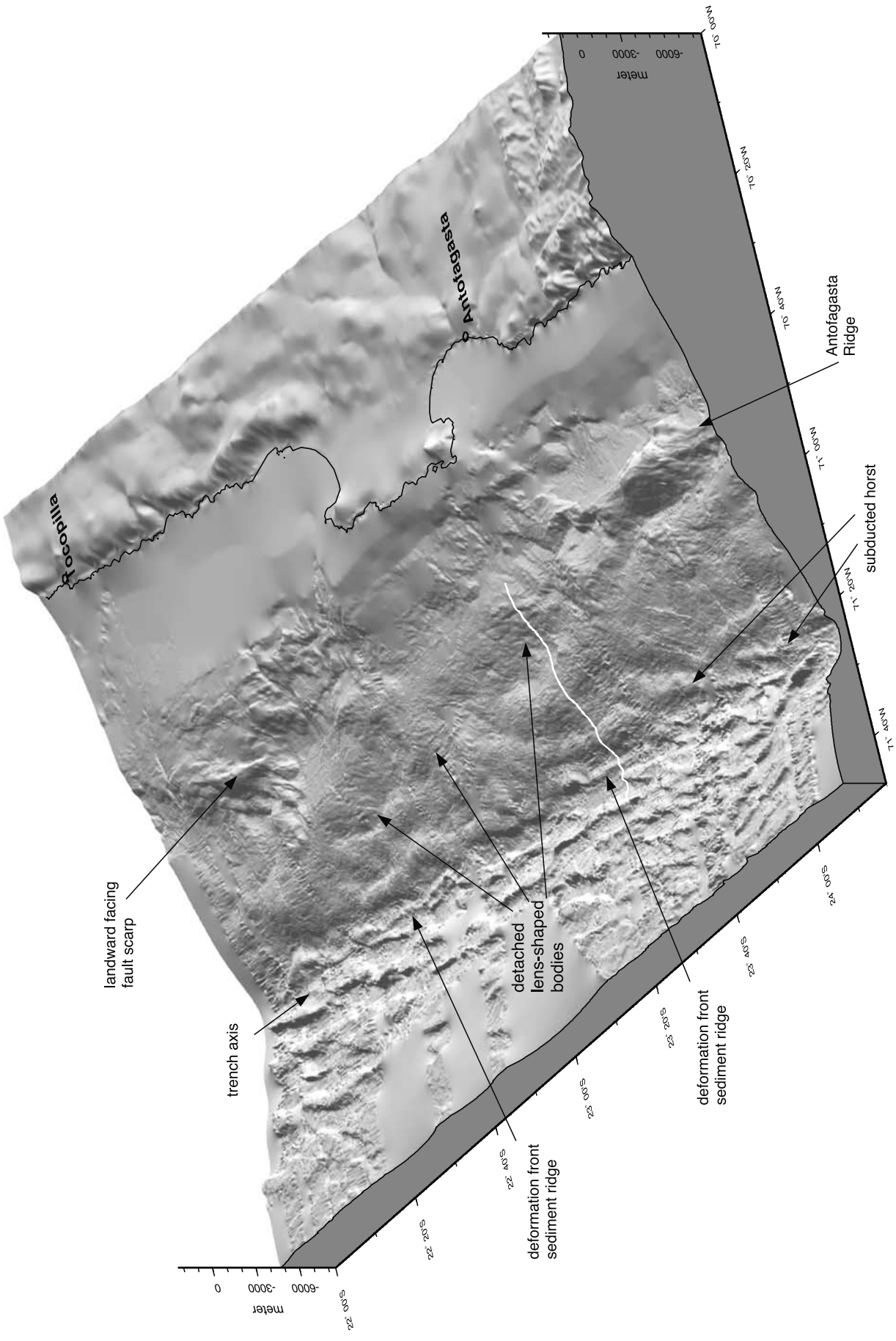

Figure 3b. Shaded relief perpspective diagram. Horst and graben morphology continues beneath the lower slope after subduction of the ocean crust. One of several large landward facing scarps is annotated.

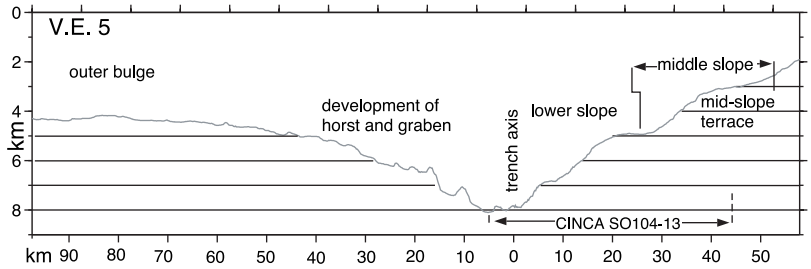

Figure 4. Bathymetric profile showing regional features and extent of SO104-13 seismic reflection record in Figure 5.

aftershocks form a linear upper surface and define the 20° dipping seismogenic zone which begins at ~20 km depth and ~45 km landward of the trench axis.

3. CINCA Data

3.1. Multibeam Bathymetry

[14] Multibeam bathymetry images deformation effectively along the northern Chile margin because it is not masked by rapid slope sedimentation. However, during CINCA the multibeam echo-sounding instrument system functioned poorly and even highly edited data remained noisy. A 2° latitude-wide corridor seaward of the 12-mile limit across the trench axis to the beginning of ocean plate flexure was mapped (Figure 2).

[15] Canyons are congruous across the upper slope although disrupted by normal faults (Figures 2 and 3) and disappear in the midslope as morphology looses sharpness and becomes smoothly undulating. This debris-smoothed morphology locally evolves into large lens-shaped bodies broken by normal fault scarps (Figures 2 and 3). Lower slope morphology reveals low ridges trending diagonal to the trench axis that overlie lower plate horsts subducted beneath the thin leading apex of the upper plate (Figures 2 and 3). Between the base of the slope and the shelf, the slope dips average 7°, but locally the upper and lower slope reach ~16°.

[16] Seaward of the trench axis, the ocean crust is disrupted by normal faulting caused by its flexure into the subduction zone (Figures 2 and 3). Faulting begins 50–65 km west of the trench axis and the crust bends downward descending 3500 m before reaching the trench axis (Figure 4). The axis of flexure crosses the northwest trend of magnetic anomalies. The anomaly trend mapped during CINCA [*Schreckenberger*, 1998] is within 10° of the pervasive fabric, clearly displayed on horsts and locally muted in the grabens (Figures 2 and 3). This fabric is inferred to be a reactivation of the faulting generated 48 Myr ago at the East Pacific Rise [*von Huene et al.*, 1999].

3.2. Seismic Reflection Acquisition and Processing

[17] The first single channel sparker seismic reflection data off the Mejillones Peninsula were acquired in 1967 [*Scholl et al.*, 1970]. Without processing, images of the sediment-basement contact on the shelf remain obscured by multiples and undefined because of vertically exaggerated steep slopes. The BGR multichannel system deployed during CINCA [*Hinz et al.*, 1995] imaged the contact locally and returned scattered reflections from within the basement. A 3000-m-long digital streamer with 120 channels recorded the signals from a 3,124 cubic inch (51.2 L) tuned air gun array. BGR data imaged normal faults across the slope and structure associated with subduction of horst and graben topography at the deformation front [*Hinz et al.*, 1998]. However, the commercially processed images do not clearly resolve deeper structure of the subduction zone. Processing of the line reported here with experimental algorithms also failed to show deep structure well [*Mann et al.*, 2000].

[18] We reprocessed and prestack depth migrated a CINCA Line (SO104 -13) [*Hinz et al.*, 1995] using iterative depth migration procedures whereby interval velocities are constrained with focusing analyses and common reflection point gathers [*Mackay and Abma*, 1993]. Coherent reflections as much as 4 km below the seafloor are sufficiently strong to give reliable velocities. Deeper velocities were further constrained with OBH wide-angle measurements [*Grotski et al.*, 1998]. With procedures different from those applied previously [*Hinz et al.*, 1998; *Mann et al.*, 2000; *Buske et al.*, 2002], basement stratification was more clearly resolved and is presented in-depth as well as in the time domain (Figure 5).

4. Tectonic Structure

4.1. Shelf and Upper Slope Structure

[19] The CINCA seismic line ends 25 km from the coast so the structure of the upper slope is known only from bathymetry and single-channel sparker paper records (Figure 6). Off the northern Mejillones Peninsula (line D4, Figure 6), a truncated structural high indicates wave base erosion and submergence of a drowned extension of the peninsula ~8 km to the north. A landward dipping normal fault with at least 250 m vertical displacement falls on a projection of the Morro Mejillones fault that vertically displaces alluvium 500 m on the peninsula [*Delouis et al.*, 1998]. In lines off the south end of the peninsula, a seaward bordering basement high indicates a 10-km continuation of the Mejillones structure (D5 and D6, Figure 6). A ~500 m (0.4–0.6 s) sediment section is observed landward of the high on the shelf. Strata are displaced at least 100–200 m seaward side up relative to the landward side across a fault cutting the outer shelf (km 10, D5, Figure 6) also reported by *Arabasz* [1971]. On the peninsula, raised paleoshorelines tilt seaward [*Hartley and Jolley*, 1995] a tilt that is repeated offshore by tilted shelf strata. Thus both onshore and offshore the data document that the Mejillones Peninsula is a

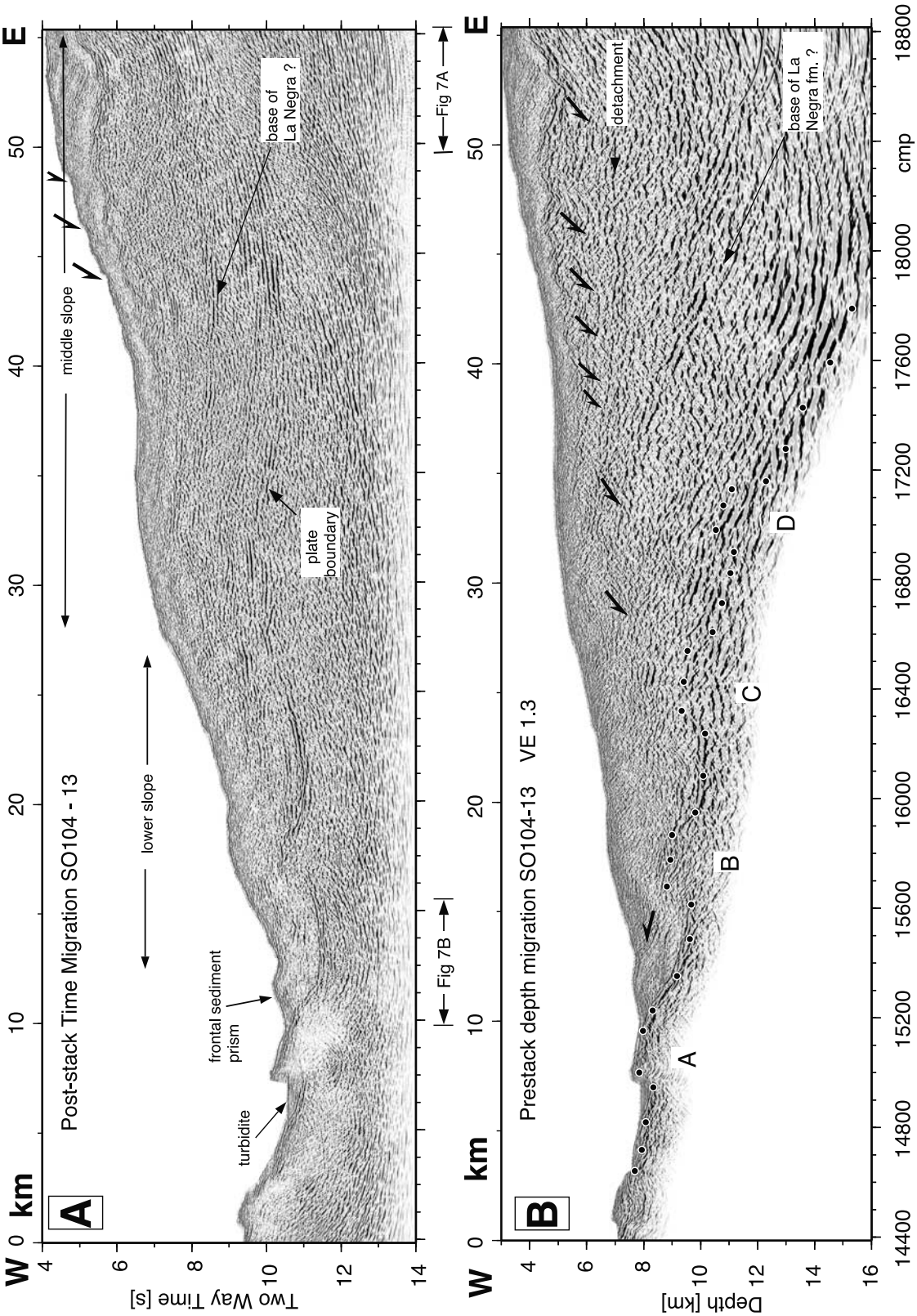

Figure 5. CINCA SO104-13 seismic images. (a) A time-migrated section and (b) the prestack depth-migrated section (vertical exaggeration is 1:3). Layering in basement is correlated with the volcanic flows of the La Negra Formation. Faults at east end of the section are imaged in the multibeam bathymetry (Figures 2 and 3). In Figure 5b, arrows indicate location of faults and dots mark igneous ocean crust surface and top of plate boundary reflective zone. Letters are keyed to the text and indicate horst in the ocean plate.

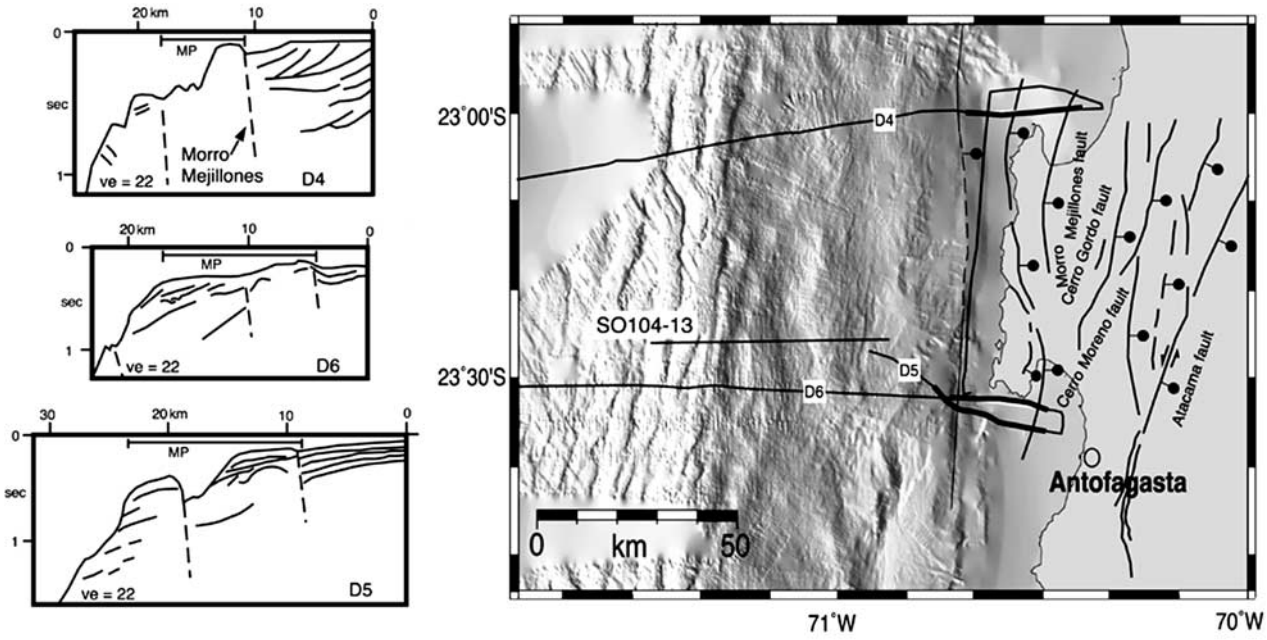

Figure 6. Interpretations of single-channel sparker seismic data acquired in 1967. Lines are located on swath-mapped bathymetry. Faults onshore are from *Delouis et al.* [1998]. MP in sections indicates the projection of the Mejillones Peninsula. Normal faults dip ~45°–60° but are drawn diagrammatically because of high vertical exaggeration.

fault block linked to landward-dipping normal faults and seaward tilted strata [*Delouis et al.*, 1998].

4.2. Middle Slope Structure

[20] The landward end of the CINCA seismic line crosses a ~3-km-deep midslope terrace (Figures 3 and 4). Beneath the terrace are five large landward rotated fault blocks (Figure 5). On the landward-most tilted block, sediment is divided into a lower ~1-km-thick sequence of parallel strata deposited prior to tilting and an upper 0.5–0.9 km section deposited during and after block rotation (Figure 7a). A canyon beginning at the shelf edge ends above the fault blocks (Figure 3). It may explain the thick upper sediment unit deposited after faulting began. Faults bounding tilted blocks extend into the basement where they end at a nearly horizontal zone of continuous reflectivity (Figure 5). These subhorizontal reflective horizons probably form a detachment beneath the sequence of rotated blocks. A similar feature was interpreted along CINCA line 13 in an ODP drill proposal by *Hinz et al.* [1998]. Restoring the tilted blocks by removing the offset of the faulted basement/sediment unconformity indicates ~4.5 km of extension and an original ~16° slope. In the restored seismic section, the lower parallel-bedded section and underlying basement unconformity at the east end of the line is near horizontal.

[21] Below the detachment, weak semicoherent basement reflections are imaged to a depth of 10 km below sea level. At the base of the upper slope (km 55, Figure 5b), they dip seaward parallel to the seafloor. Seaward beneath the lower midslope (km 30–35, Figure 5b), basement reflections dip landward paralleling the underlying plate boundary. We infer that a high-amplitude reflection is the base of the Jurassic La Negra Formation and that overlying reflections represent volcanic layering (Figure 5). The La Negra overlies Jurassic and Triassic granitoids and Paleozoic metamorphic rock.

4.3. Lower Slope Structure

[22] In the CINCA seismic line, the trench axis is ~8 km deep and has a flat seafloor <1-km-wide underlain by a small turbidite wedge <200 m thick (Figure 5). The trench axis is bordered landward by a steep scarp striking somewhat diagonal to the line of section (Figure 3). It forms the seaward fault scarp of horst A that enters the subduction zone (Figure 5b). The downdip graben (A–B, Figure 5b) is completely filled with stratified detritus 1-km-thick folded and offset by an axial thrust (km 11–15, Figure 7b). This fold forms the deformation front which is a seafloor ridge parallel to the trench axis rather than the trend of the horst (Figures 2 and 3). The seaward-facing scarp of the adjacent and subducted horst B (Figure 5b) is poorly imaged but the clear landward facing one is 1 km high. The to of subducted horst C (Figure 5b) is almost at a depth of 10-km below sea level and its crest is traced by one of two strong reflections. Subducted horsts have twice the relief of unsubducted horsts. The crest of horst C (Figure 5b) comes within 1.5–2 km of the lower end of a normal fault plane reflection under the seaward edge of the midslope (km 30, Figure 5). This constrains the zone across which contractile and extensional strain is separated. The dip of the subducting ocean crust increases only slightly for 20 km downdip from the trench axis and then steepens abruptly to 18° landward of D (Figure 5b). We joined a line from the top of ocean crust at point C (Figure 5) with the updip end of the seismogenic zone identified at the landward end of the line

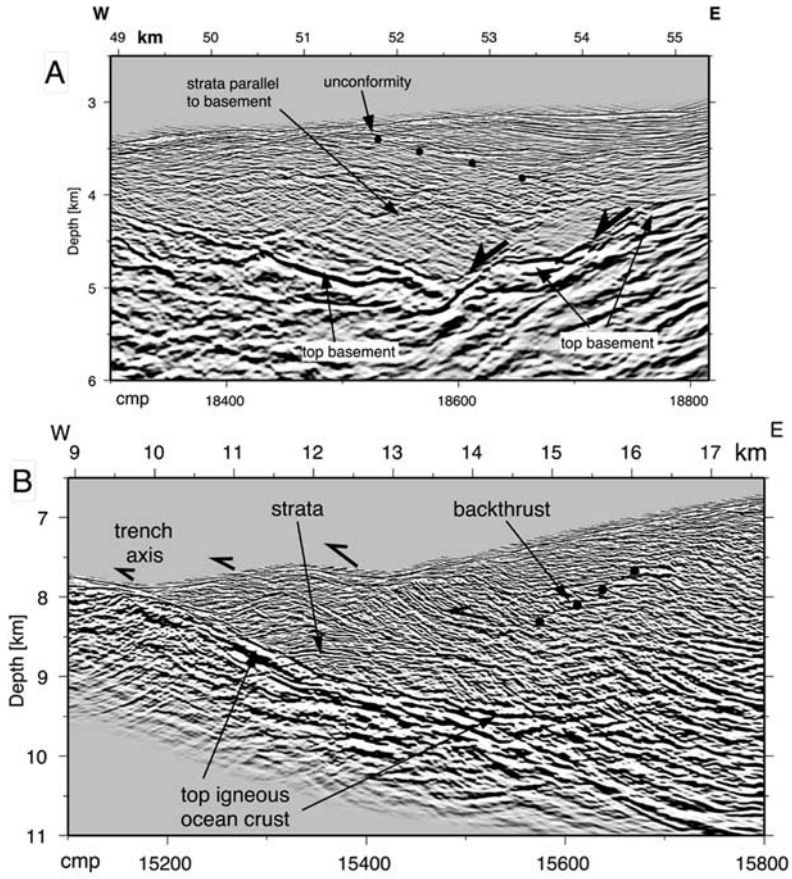

Figure 7. Large-scale depth images without vertical exaggeration. (a) A section on upper midslope fault block, and (b) the base of slope. Location along the seismic record is shown in Figure 5.

by *Husen et al.* [2000]. This line dips 20° and is steeper than the 15° derived from refraction modeling of air gun shots recorded onshore [*Patzwald et al.*, 1999]. These authors assumed an abrupt point of inflection at the trench axis. If the point of inflection were modeled at point C (Figure 5), the dips agree. Velocities from prestack migration are reliable to the depth of inflection, an observation that gives us confidence it occurs there. Flexure of the subducted ocean crust beneath the slope is greater than flexure in the 65 km seaward of the trench axis. The significance of flexure beneath the midslope is discussed below.

[23] A strong or continuous reflector that marks the plate boundary thrust extends between horsts B and C (Figure 5b). Reflections above these two elevated blocks indicate uplift and contractile deformation of the overlying acoustically stratified section consistent with the profile of seafloor ridges and depressions over subducted horst and graben relief. Landward of point C (Figure 5b) a 1.5-km-thick zone of low-frequency reflections arches over the horst and continues parallel to the 20° dipping ocean crust. This reflective plate boundary image is similar to that exhibited along many sedimented convergent margins.

[24] Velocities determined during prestack depth migration decrease significantly from the middle to the lower slope as was also observed during seismic processing to produce time sections [*Hinz et al.*, 1998]. Reflections within the basement of the upper plate loose amplitude beneath the lower slope and the once coherent basement unconformity fragments. The reflectors below it become obscure and merge with the nearly structureless reflectivity of the frontal prism (Figure 5).

5. Discussion

5.1. Interpretation of Structure

[25] North of the Mejillones Peninsula, the Coastal Cordillera is prominent (Figure 2), however, the peninsula is a separate structural high positioned to the west near the shelf edge. Several authors have inferred that the peninsula is bordered offshore by seaward dipping normal faults [i.e., *Armijo and Thiele*, 1990], and they were proposed in an earlier interpretation of multibeam seafloor morphology [*von Huene et al.*, 1999]. Even though landward dipping normal faults were shown to predominate onshore, a seaward dip was inferred offshore [i.e., *Delouis et al.*, 1998]. However, in single-channel seismic images across the upper slope, offshore faults exhibit a persistent down-to-the-east vertical displacement and fault blocks tilt seaward (Figure 6). Reexamining the multibeam bathymetry north of Mejillones Peninsula shows several landward facing scarps along the upper slope (Figure 3b). Landward dipping faults were also interpreted where other CINCA lines approach the shelf edge [*Block*, 1998]. Although the depth of the faults is not constrained in available seismic records, the 25 to 65 km

length of the scarps indicates a vertical extent to midcrustal depth.

[26] To explain extensional faulting of the northern Chile margin, investigators have proposed stretching of the upper plate over a subducted ridge or local underplating. *Hartley and Jolley* [1995] proposed subduction of a branch from the Iquique Ridge beneath the Mejillones Peninsula and the 1995 earthquake rupture began just east of the peninsula suggesting a subducted asperity there [*Delouis et al.*, 1998; *Husen et al.*, 2000]. However, 3-D tomography indicates no subducted feature of anomalous velocity with a planform like the peninsula [*Husen et al.*, 2000]. The subducting Nazca Ridge off Peru and the Cocos Ridge colliding with Costa Rica are each associated with peninsulas similar to Mejillones but the underthrusting ridges are much larger than Iquique Ridge let alone a branch from it [*von Huene et al.*, 1996, 2000]. Underplating and thus uplifting the peninsula [*Delouis et al.*, 1998; *von Huene et al.*, 1999] requires a mechanism locally isolating this process for 2 Myr, or during the subduction of 180 km of lower plate. Furthermore, the low-velocity body thought to correspond with underplated material [*Husen et al*, 2000] lies seaward of the peninsula and trends normal to it. Underplating from unbending of the downward flexed lower plate beneath Mejillones Peninsula is not supported by the plate boundary defined by the 1995 earthquake aftershocks [*Husen et al.*, 2000; *Buske et al.*, 2002].

[27] As an alternative explanation, the peninsula could represent a seaward tilted block in which the block's landward edge is emergent. Transverse fault zones (Figure 3) truncate the north and south ends of the block. Rotation would result in the slow uplift of a narrow 85-km-long footwall ridge as the area is flexurally faulted along landward dipping normal faults [*Buck*, 1988]. The submerged Antofagasta Ridge (Figures 2 and 3) is of the same size and morphology as Mejillones Peninsula. Its seaward dipping strata indicate a seaward tilted block [*Block*, 1998]. North of the peninsula is another ridge with a landward facing scarp that could be a tilted block in the process of breaking up at the midslope. Mejillones may be unusual in being the only such ridge above sea level. Its separation from the Coastal Cordillera (Figure 2) suggests a separate tectonic structure. None of the explanations for the height of the peninsula are well constrained by data; however, the steady uplift of an elongate ridge over 2 Myr is most consistent with gradual block rotation during flexural faulting (Figure 8).

[28] Faulting and seaward tilting of blocks across the upper slope contributes to break-up and gravity failure of the steepened seafloor. Debris shed from the fault blocks presumably produces the ~500-m-thick detritus that covers the middle slope. In the middle slope, faulting is gravity driven as observed across the 30-km-wide detached oval body (Figures 3 and 5, km 35–55). At km 30 (Figure 5), the extended upper plate converges with detritus draped over relief on the subducting plate. The morphology of the middle slope reflects gravity-driven upper plate tectonism whereas down slope the morphology mimics that of the subducted relief on the buried lower plate (Figures 2 and 3).

[29] The lower slope frontal prism facilitates subduction of slope detritus in underthrusting grabens. If the subducting grabens are filled at the deformation front (Figure 7b), then the lower slope ridges and valleys must be caused by the continued growth of graben relief after subduction as observed in the depth image (Figure 5). The paleospreading ridge fabric crossing the horst and grabens must also continue to grow since it is traced across the trench in some displays of the lower slope multibeam bathymetry (Figures 2 and inset of Figure 6). The dip of the subducting plate increases slightly underneath the lower slope and then steepens rapidly to 20° at km 35 beneath the middle slope (Figure 5b). The sharp middle slope flexure of the lower plate corresponds with upper plate fragmentation by faulting. Despite growth of subducted graben, the overlying lower slope detritus contains minor contractile structures linked to plate convergence and down slope gravity sliding. Plate boundary thrusts are imaged from the deformation front at the base of the slope about 20 km landward. At greater subsurface depth the plate boundary is no longer imaged as a single reflection and is located somewhere within a 1.5-km-thick layer characterized by three to five reflections. This zone of multiple reflectors is imaged from the middle slope to a subsea level depth of 15 km where the seafloor multiple obscures primary arrivals.

5.2. A Model

[30] Our interpretation of structure in the corridor containing the Mejillones Peninsula is diagrammed in Figure 8 and we propose the following kinematic model. From the Atacama Fault (Figure 6) across the shelf and upper slope, landward dipping faults become dominant and isolate blocks that tilt to form a ''domino'' structured extensional framework. Shelf strata are tilted as much as 15° on the seaward-most fault blocks beneath the upper slope (Figure 6). This ''domino'' structure could result from a loss of lateral support as the lower and middle slopes are removed by subduction erosion (Figure 8, insert). Fault block tilting steepens the upper slope, and blocks also subside down slope as they are undermined by basal erosion. In the middle slope, gravity tectonics intensifies and massive lens-shaped bodies locally detach along subhorizontal faults deep in the continental basement. Extension within the detached bodies fragments them and contributes to mass wasting. The midslope rock framework is weakened and beneath the lower slope, basement disaggregation becomes severe. The tectonized material becomes acoustically indistinguishable from mass wasted slope debris piled up at the base of the slope. Debris at the base of slope fills the underthrusting grabens, and as they subduct beneath the frontal prism, the elevation of pore fluid pressure reduces friction along the plate interface and along faults in the underlying subducted plate. Perhaps reduction of friction along normal faults cutting the ocean plate releases residual flexural stress and increases its relief. Overpressured fluid from the lower plate permeates the underside of the upper plate weakening it and disaggregating the lowermost rock into a mass of fragments that can be transferred to the enlarging underthrust graben. This action undermines the middle slope and steepens the overlying seafloor thereby accelerating mass wasting.

[31] The observations on which our model is based are similar to those observed along the sediment-starved Tonga margin. From ODP drill cores, *Clift and MacLeod* [1999] have documented progressive trenchward tilting of the slope that is ascribed to subduction erosion. Growth of subducted

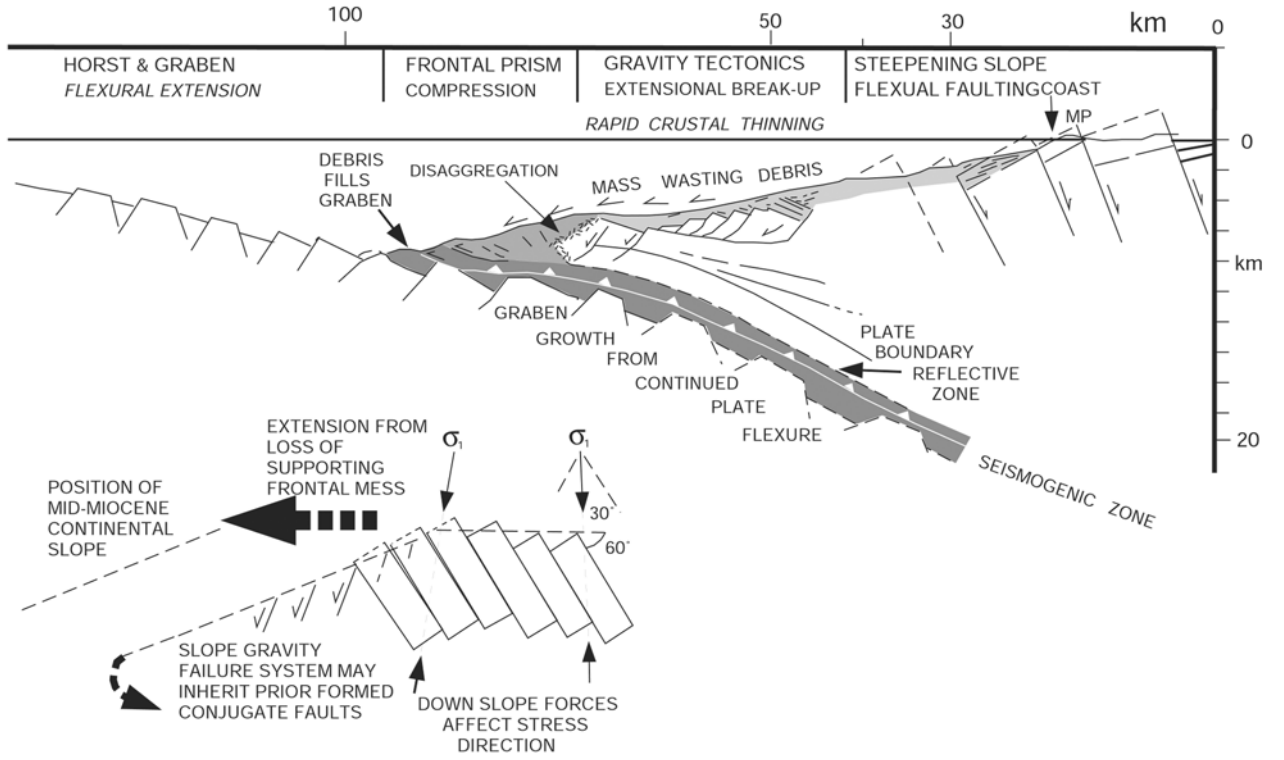

Figure 8. A tectonic model to explain Quaternary subduction erosion across the seismic transect. Solid lines are observed and dashed lines are inferred structure. On-land structure is after *Delouis et al.* [1998] with peninsular relief inferred as the high edge of a tilted block (MP). Inset shows proposed domino extensional structure from loss of the frontal supporting mass through erosion. Sigma 1 on land is from *Delouis et al.* [1998], and at shelf edge it is inferred. Rapid upper plate crustal thinning is centered about the middle slope where the continued growth of grabens is associated with lower plate crustal flexure. Here the upper plate is thin enough to break up, whereas beneath the upper slope it remains coherent. The plate boundary reflective zone is interpreted as consisting of subducting clastic debris.

graben was interpreted in a seismic depth image across the Tonga Trench [*von Huene and Scholl*, 1991, Figure 7]. The filling of graben with slope debris off northern Chile is not only similar to that observed along the Tonga margin [*Balance et al.*, 1989] but also the Japan margin [*von Huene and Culotta*, 1989] and the Aleutian Trench [*McCarthy and Scholl*, 1985].

5.3. Location of Subduction Erosion

[32] Although erosional structure along the base of the upper plate is acoustically unresolved, previous investigators [*von Huene and Scholl*, 1991; *Hinz et al.*, 1998], noted that basal erosion must be a dominant process otherwise lower crustal rock would crop out at the trench. We develop this point below.

[33] The upper slope blocks that have tilted seaward and migrated down slope retain part of their sediment cover (Figure 3 between 22°20′ and 22°40′S and Figure 6, D5, and Figure 7a). These sediment sections were probably deposited on the shelf when the underlying unconformities were also more horizontal. The parallel strata on basement in the seismic images are structurally similar to the Miocene shelf sediment unconformably deposited on basement and locally exposed on land [*Hartley and Jolly*, 1995]. Strata capping the upper slope basement blocks displaced seaward from the shelf (Figure 3) and the buried parallel strata on the uppermost detached and tilted midslope fault block are most likely shelf deposits also (Figure 7a). Restoring normal fault displacement of the midslope detached body recreates a near horizontal basement surface consistent with wave base erosion. If a former shelf has subsided to 4 km depth, we suggest that roughly this amount of basal erosion must have occurred because 4 km of seafloor erosion would have removed the shelf sediment cover.

[34] Continuation of the buried unconformity beneath inferred shelf deposits across the midslope indicates massive subsidence of an eroded paleoseafloor. The middle slope appears to be a locus of enhanced basal erosion here and along other margins. Erosional unconformities at great depth are found beneath the midslope along the Peru and Middle America trenches [*von Huene et al.*, 1988; *Ranero and von Huene*, 2000; *Ranero et al.*, 2000; *Vannucchi et al.*, 2001], Japan [*von Huene and Cullotta*, 1989], and Tonga margins [*von Huene and Scholl*, 1991].

5.4. Rates of Erosion

[35] Subduction erosion along the north Chile margin was previously estimated [*von Huene and Scholl*, 1991; *Scheuber*, 1994], but those rates were averaged over much of Tertiary time. Estimates of erosion were made based on current

graben volume [*Hinz et al.*, 1998; *von Huene et al.*, 1999]. The seismic depth section provides a better cross section of grabens at the deformation front compared with time-based profiles used in previous estimates. Grabens entering the subduction zone are 5 to 6 km wide and 0.5 km deep (Figure 4), and 11–12 grabens occur across the 95 km of ocean crust subducted per million years. Thus for each km of trench, the underthrusting grabens have a capacity to transport 28–36 km^3/Myr of slope material down the subduction zone. To compare the volume of eroded with solid upper plate material, the pore water in the detrital graben fill must be subtracted. Assuming an average 30% porosity the dry volume of fill is 36–47 km^3/Myr. The capacity of graben growing beneath the upper plate doubles after subduction for a total of 72–94 km^3/Myr/km of margin. This estimated capacity of grabens is much greater than the long-term average of 37–50 km^3/Myr erosion derived from volcanic arc migration [*Scheuber*, 1994].

[36] Another estimate of erosion involves the sediment deposited parallel to basement that is now under the mid-slope (Figure 7a). If the basal beds of this sequence were deposited on the shelf, then this former shelf area has subsided ~4 km in the past 20 Myr. This is consistent with the 16 Miocene (~20 Ma) samples recovered from 500 to 5000 m depth because they are not described as deep-water deposits [*Bandy and Rudolfo*, 1964; *Scholl et al.*, 1970; *Kudrass et al.*, 1998]. A sample recovered from deep water north of Mejillones was clearly once at neritic depth [*Kudrass et al.*, 1998]. If the parallel strata are shelf deposits, the shelf edge has retreated 25–35 km in ~20 Myr, or equivalent to an erosional rate of 45–50 km^3/Myr and within the long term limits indicated by arc migration [*Scheuber*, 1994].

[37] A graben capacity in excess of other estimated erosional volumes was also found along the Tonga margin [*Balance et al.*, 1989]. Balance et al. explained this discrepancy with the contribution to graben fill of arc derived volcanic sediment and pelagic sediment in addition to the material eroded from the upper plate. A similar explanation might apply along the northern Chile margin as indicated by the sediment sampled from the slope [*Kudrass et al*, 1998]. However, without a better understanding of sediment composition and distribution, a volumetric estimate of upper plate material eroded during Neogene time is poorly constrained.

5.5. Erosion and Basal Friction

[38] Erosion along the sediment-starved northern Chile margin has been presumed to involve high basal friction based on morphology [*Jarrard*, 1986], seismicity [*Uyeda and Kanamori*, 1979] and on wedge taper analysis [*Adam and Reuther*, 2000]. High basal friction is inconsistent with indications that traction beneath the middle and lower slope is similar to that along sedimented margins with matching rates of convergence. It is also inconsistent with the severe weakening of the rock framework beneath the middle slope because weak rock cannot support high friction. Indications that interplate coupling is comparable to sediment dominated margins where coupling is thought to be weakened by pore water include:

1. The ~1.5-km-thick subducting layer of clastic debris contains fluid amounts comparable to sedimented margins. With velocity/porosity diagrams [*Erickson and Jarrard* 1998], this comparison can be quantified. Clastic material of the first ridge pushed up by a subducting graben at the deformation front has a velocity from 1.8 km/s near the surface to 2.8 km/s at 1 km depth. These velocities indicate a porosity of ~40% at the surface to ~20% at the base. After subduction of 1 km the same section has a 20% porosity in shale and a 30% porosity in sandstone [*Erickson and Jarrard*, 1998]. Velocity/porosity conversions at the Peru and Aleutian trenches average around 30–35% and the frontal prism drilled off Costa Rica has acoustic velocities of 1.6–2.2 km/s and 55%–60% porosity [*Kimura et al.*, 1997]. Pore pressure is also elevated [*Lallemand et al.*, 1994; *Saffer et al.*, 2000]. Additionally, the fracture permeability along faults cutting ocean crust off Antofagasta is exposed directly to seawater before subduction thus facilitating invasion of fluid that might be later expelled into the interplate boundary. Postseismic fluid flow along the plate boundary beneath the Mejillones Peninsula explains time evolution of seismic velocities [*Husen and Kissling*, 2001].

2. In the upper plate, normal fault plane reflections extend down to the 1.5-km-thick reflective zone containing the plate boundary and define a narrow transition from contractile to extensional strain, consistent with weak coupling.

3. If basal subduction erosion is a high friction process, high interplate seismicity would be expected beneath the middle slope where basal erosion is most active, however, seismicity is low. In fact, the updip end of the northern Chile seismogenic zone is 5–7 km deeper than that indicated by aftershocks following the great 1985 earthquake along the heavily sedimented margin off Valparaiso [*Comte et al.*, 1986]. That seismicity clusters around the plate boundary observed in seismic refraction sections indicating association with the seismogenic rupture plane [*Flueh et al.*, 1998; *Hojka et al.*, 2000]. South of Juan Fernandez Ridge (Figure 1) the trench axis contains 2.5-km-thick turbidites of which 1.6 km is subducted [*von Huene et al.*, 1997; *Flueh et al.*, 1998]. The location of the updip end of the northern Chile seismogenic zone indicates no stronger coupling off Antofagasta than along accreting segments of the Chile margin.

[39] Re-evaluating inputs to the taper analysis of *Adam and Reuther* [2000] helps resolve conflicting estimates of interplate friction. They presumed rock strength measured at the KTB drill site (Continental Deep Drill-hole) and applied it to the entire width of the continental slope. They applied the lower plate boundary dip from refraction data recorded on land. From the depth migrated seismic image, we find that material strength is lower, the taper of the frontal prism is complex, and pore pressure appears higher than they assumed. Supporting observations are as follows:

[40] For material strength, the depth section (Figures 5 and 7a) allows quantitative analysis from angular relations based on Coulomb criteria [*Dahlen*, 1984; *Davis and von Huene*, 1987]. Structural relations of the conjugate forethrust, backthrust, and the decollement yield material strength ($\mu = \tan\theta$) and traction [*Lallemand et al.*, 1994]). Measurements were limited to the first thrust slice of the prism to avoid faults rotated during thrusting of subsequent thrust slices (forethrust $\delta_f = 29°$, backthrust $\delta_b = 33°$). The strength ($\mu = 0.51$), is comparable with the averaged

strength ($\mu = 0.52 \pm 0.10$) of *Lallemand et al.* [1994] in the frontal region of accretionary prisms and much less than the strength ($\mu = 0.7$) of KTB measurements. To quantify strength of the middle slope, the detached body was analyzed using the methods for slide failure of *Watts and Grilli* [2002]. The averaged basal friction 3.8 MPa is about 1/2 the average shear strength of consolidated marine sediment despite its path through basement (P. Watts, written communication, 2001). It indicates a weak upper half of the midslope basement showing the appropriateness of applying a low strength in taper calculations to at least the upper slope.

[41] For taper, the seaward taper of the lower slope imaged in the seismic section agrees with the measured seafloor slope α and the assumed plate boundary dip β of *Adam and Reuther* [2000]. But beneath the middle slope the plate boundary is nonplanar and dips change rapidly precluding simple taper analysis. Averaging taper across the entire continental margin to the updip end of the seismogenic zone gives questionable results.

[42] For pore pressure, to subduct fresh mass-wasting debris beneath older debris deposits of the frontal prism requires a level of basal friction similar to that reported by *Lallemand et al.* [1994] for accretionary margins. Basal friction is commonly considered approximately equivalent to material strength. The analysis for material strength from conjugate faults mentioned above yielded a pore pressure about 90% of lithostatic as in the Aleutian accretionary prism [*Davis and von Huene*, 1987]. However, this estimate includes only the first 2.5-km of the prism which is shorter than the segments compiled by *Lallemand et al.* [1994].

[43] The taper of the Antofagasta frontal prism is plotted with other tapers assuming the average strength and pore fluid pressure of frontal prisms of *Lallemand et al.* [1994] (Figure 9). Subsequent to the compilation of *Lallemand et al.* [1994], many precisely measured tapers have become available from depth processed images and coincident OBH/S seismic refraction transects. The tapers used here span only the frontal prism and a small part of the adjacent backstop. Central and South American tapers cluster in the area of Lallemand et al.'s intermediate group and are distant from his nonaccretionary field (Figure 9). Clustering indicates similarity notwithstanding inclusion of some well-sedimented margins. The Antofagasta taper plots at the nonaccretionary end of the cluster, essentially on the Peruvian 12°S tapers [*von Huene et al.*, 1996]. The lower four Chilean tapers are from margins with ~15-km-wide prisms [*Diaz-Naveas*, 1999]. Costa Rican tapers associated with the erosive impact of the Cocos Ridge and its associated seamounts (three upper triangles, Figure 9) plot close by whereas those opposite a smooth subducting plate are in the stable wedge field [*Ranero and von Huene*, 2000]. Of the two Guatemalan tapers, the one from the DSDP drill transect [*Ambos and Hussong*, 1985] is without a significant frontal prism and perhaps was recently impacted by a subducting seamount explaining its greater taper. The grouping of intermediate tapers supports our inference that many conditions at the front of sediment-starved and well-sedimented segments of the Chilean margin are similar.

[44] If abrasion in a high basal friction environment is an unlikely mechanism of erosion, then what process removes material from the underside of the upper plate? As discussed before, a possible mechanism involves subsurface enlargement of subducted grabens. Off Antofagasta, tectonic stopping of material can fill the increased graben volume. Hydrofracturing by fluids in subducting grabens is inferred to fragment rock along the base of the upper plate that is then transferred into lower plate graben. Upper plate thinning by basal erosion above grabens and differential compaction of graben fill is indicated by seafloor subsidence along shallow valleys above the grabens subducted beneath the lower slope.

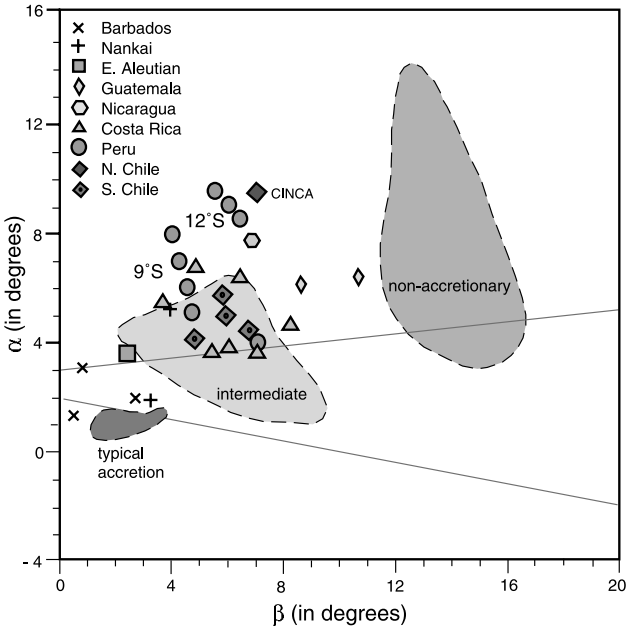

Figure 9. A taper stability plot of α versus β [after *Lallemand et al.*, 1994] for the lower and middle slopes of margins imaged with depth processed seismic reflection and OBS/H transects. Only the taper of the frontal prism and small parts of the backstop are included. Tapers are from Central America to southern Chile north and south of the CINCA line. The Barbados, Nankai, and Aleutian margins represent accretionary margins. In the Chilean tapers, the lower four are along sediment flooded segments with smaller α to compare with the CINCA taper. Peru at 12°S (upper sequence) is just north of the subducting Nazca Ridge, and 9°S (lower sequence) where accretion has stabilized. The upper three Costa Rican tapers are affected by subduction of Cocos Ridge. The two Guatemalan tapers are from a reprocessed Exxon reflection line (*Seely et al.* [1974], reprocessed at Geomar) which has a frontal prism (left diamond), and OBS refraction data without a prism (DSDP drill transect) where recent erosion from subduction of a seamount is suspected. Shaded fields are those of *Lallemand et al.* [1994] and the gray lines outline their accretionary stability field.

5.6. Global Implications

[45] In the spectrum of convergent margins, the northern Chile Margin is the high-stress end-member in the often-cited classification of *Uyeda and Kanamori* [1979] and a highly compressional end-member in the scheme of *Jarrard*

[1986]. Although the structure assumed 20 years ago is revised significantly with subsequent observations, this margin has all the characteristics that combine to produce high basal friction [see *Lallemand et al.*, 1994]. For example, subducting topography is rough, trench sediment insignificant, and the upper plate is composed of crystalline continental rock. Twenty years ago, concepts were explored to explain subduction erosion such as (1) the role of horst and graben roughness, (2) upper plate strength, and (3) the elevation of pore fluid pressure. These concepts are revisited below.

1. The graphic roughness of the subducting plate as commonly portrayed is misleading because the horst and graben relief is levelled at the deformation front by sediment and clastic materials. This levelling removes upper plate material and gives rise to frontal erosion. The enlargement of subducted graben can accommodate loose material from hydrofracturing of the backstop thereby facilitating basal erosion. Tectonic thickening of slope sediment or accretion at the deformation front can be coeval with erosion of the underside of the prism farther down the subduction zone as previously suspected [i.e., *Lallemand et al.*, 1994]. A balance between addition and subtraction of mass stabilizes the size of a frontal prism.

2. Elevated pore pressure controls tectonic processes beneath the continental slope, by reducing friction and weakening the upper plate. Permeable basement faults aid fluid migration that decreases upper plate rigidity to levels nearing those of accretionary margins. In our view, strength of the upper plate is more a function of fracturing and hydration rather than composition.

3. Subducted slope detritus appears to be as porous as trench turbidites. Additional fluid is contained in fractured ocean crust. The subduction of ocean floor sediment sequences is not essential to subduction zone overpressure along rapidly converging margins.

6. Summary and Conclusions

[46] Geophysical and geologic data across the sediment-starved Antofagasta convergent margin of northern Chile reveals dominantly extensional tectonics. The landward dipping normal faults onshore continue offshore to form a 75- to 100-km-wide seaward verging "domino type" structural domain. In the middle slope, seaward dipping normal faults sole into a near horizontal basement detachment reaching a depth of 4 km below the seafloor. Restoring the detached mass indicates 4.5 km of extension and a steep predetachment seafloor. In three dimensions, the detached mass is a 35 $\times$ 20 km lens-shaped body that thins by extension down slope and disintegrates by mass wasting. A $\sim$500-m cover of debris from mass wasting and coastal erosion smoothes topography. Disintegration of the continental rock framework supplies the trench axis with sufficient slope debris to overwhelm horst and graben relief on the converging ocean crust. Grabens are filled prior to subduction, and excess detrital debris locally overthrusts the horsts. Lower plate relief is levelled at the base of the slope and low seismic velocities indicate abundant fluid input to the plate boundary. The plate interface thrust fault cuts through these clastic materials. Another potential fluid source is from hydrated fractures in the subducting ocean plate that were exposed directly to seawater.

[47] Seaward of the trench axis, flexural extension in the oceanic plate produces grabens that reach an average 0.5 km depth at the base of the slope. Once the plate is subducted, further fault displacement enlarges the graben relief. A probable cause is the increased plate flexure and elevated fluid pressure beneath the frontal prism. Subsurface graben deepening and differential compaction produce shallow valleys in the overlying lower slope seafloor and provide a sink for upper plate material. We conclude that lower plate relief formed in the subduction zone probably accommodates material detached from the upper plate.

[48] The reflection seismic image resolves the plate interface thrust fault for a distance of $\sim$20 km beneath the lower slope and farther downdip it passes into a 1.5-km-thick reflective zone. The partitioning of compression and extension occurs close to the reflective zone and indicates weak coupling and little transmission of compressional stress into the upper plate. The updip end of the seismogenic zone is deeper and farther from the trench axis than observed along the sedimented flooded trench axis south of Valparaiso. Apparently the northern erosional environment involves levels of basal friction, pore pressure, and upper plate strength similar to that found in the sedimented southern Chile margin.

[49] Most well imaged erosional margins have a small frontal prism that elevates pore pressure and facilitate subduction of sediment. The prism is ephemeral and can be composed of accreted trench turbidites and/or of remolded slope deposits that have collected near the deformation front and been deformed. Examples are the erosional margins of northern Japan, [*von Huene et al.*, 1994; *Tsuru et al.*, 2000], Peru [*von Huene and Lallemand*, 1990], Guatemala, Nicaragua [*Ranero et al.*, 2000], and Costa Rica [*von Huene et al.*, 2000; *Ranero and von Huene*, 2000; *Vannucchi et al.*, 2001]. These frontal prisms are underlain by subducting sediment. Environments of erosion and accretion may differ more in subducted plate flexure and rates of convergence than in coupling.

[50] **Acknowledgments.** We are grateful to our colleague Dirk Klaeschen for assistance in processing, to Karl Hinz and Christian Reichert for releasing the CINCA seismic data, to David Scholl for making single-channel data available and his helpful review, to Serge Lallemand for discussions, and to reviewer Yoshitaka Hashimoto for his comments.

References

Adam, J., and C.-D. Reuther, Crustal dynamics and active fault mechanics during subduction erosion: Application of frictional wedge analysis on to the North Chilean Forearc, *Tectonophysics*, *321*, 297–325, 2000.

Ambos, E. L., and D. M. Hussong, Structure at the toe of the subduction complex: Middle America Trench offshore Guatemala, *Initial Rep. Deep Sea Dril.l Proj.*, *84*, 816–878, 1985.

Arabasz, W. J., Geological and geophysical studies of the Atacama fault zone in Northern Chile, Ph.D. thesis, Calif. Inst. of Technol., Pasadena, 1971.

Armijo, R., and R. Thiele, Active faulting in northern Chile: ramp stacking and lateral decoupling along a subduction plate boundary?, *Earth Planet. Sci. Lett.*, *98*, 40–61, 1990.

Balance, P. F., D. W. Scholl, T. L. Vallier, A. J. Stevenson, and H. Ryan, Subduction of a late Cretaceous seamount of the Louisville Ridge at the Tonga Trench: A model of normal and accelerated tectonic erosion, *Tectonics*, *8*, 953–962, 1989.

Bandy, O. L., and K. S. Rudolfo, Distribution of foraminifera and sediments, Peru-Chile Trench area, *Deep Sea Res.*, *11*, 817–837, 1964.

Block, M., Interpretations of MCS data, in *Crustal investigations off- and onshore Nazca/Central Andes* (*CINCA*), coordinated by K. Hinz and members of the CINCA Study Group, *Rep. BGR 117.613*, pp. 69–102, Bundesanst. für Geowis. und Rohstoffe, Hannover, Germany, 1998.

Buck, W. R., Flexural rotation of normal faults, *Tectonics*, *7*, 959–973, 1988.

Buske, S., H. Meyer, S. Luth, R. Patzig, C. Reichert, S. Shapiro, P. Wigger, and M. Yoon, Broad depth range seismic and seismological imaging of the subduction processing North Chile, *Tectonophysics*, *350*, 273–282, 2002.

Clift, P. D., and C. J. MacLeod, Slow rates of subduction erosion estimated from subsidence and tilting of the Tonga forearc, *Geology*, *27*(5), 411–414, 1999.

Comte, D., A. Eisenberg, E. Lorca, M. Pardo, L. Ponce, R. Saragoni, S. K. Singh, and G. Suárez, The 1985 central Chile earthquake: A repeat of previous great earthquakes in the region?, *Science*, *233*, 449–453, 1986.

Couch, R., R. Whitsett, B. Hehm, and L. Brucerno-Guarupe, Structures of the continental margin of Peru and Chile, *Mem. Geol. Soc. Am.*, *154*, 703–726, 1981.

Dahlen, F. A., Noncohesive critical Coulomb wedges: An exact solution, *J. Geophys. Res.*, *89*, 10,125–10,133, 1984.

Davis, D. M., and R. von Huene, Inferences on sediment strength and fault friction from structures of the Aleutian Trench, *Geology*, *15*, 517–522, 1987.

Delouis, B., et al., The M_w = 8.0 Antofagasta (northern Chile) earthquake of July 30, 995, a precursor to the end of the 1877 gap, *Bull. Seismol. Soc. Am.*, *87*(427), 445, 1997.

Delouis, B., H. Philip, L. Dorbath, and A. Cisternas, Recent crustal deformation in the Antofagasta region (northern Chile) and the subduction process, *Geophys. J. Int.*, *132*, 302–338, 1998.

Diaz-Naveas, J. L., Sediment subduction and accretion at the Chilean convergent margin between 35° and 40°S, Ph.D. dissertation, 130 pp., Christian-Albrechts-Univ., Kiel, Germany, 1999.

Erickson, S. N., and R. D. Jarrard, Velocity-porosity relationships for water-strurated siliciclastic sediments, *J. Geophys. Res.*, *103*, 30,385–30,406, 1998.

Fisher, R. L., and R. W. Raitt, Topography and structure of the Peru-Chile trench, *Deep Sea Res.*, *9*, 423–443, 1962.

Flueh, E. R., N. Vidal, C. R. Ranero, A. Hojka, R. von Huene, J. Bialas, K. Hinz, D. Cordoba, J. J. Dañobeitia, and C. Zelt, seismic investigation of the continental margin off- and onshore Valparaiso, Chile, *Tectonophysics*, *288*, 251–263, 1998.

Grotski, N. R., E. R. Flueh, C. J. Reichert, R. Patzwahl, J. Mechie, and P. Giese, Modelling of seismic wide-angle/refraction data, *Crustal investigations off- and onshore Nazca/Central Andes* (*CINCA*), coordinated by K. Hinz and members of the CINCA Study Group, *Rep. BGR 117.613*, 69–102, Bundesanst. für Geowis. und Rohstoffe, Hannover, Germany, 1998.

Hartley, A. J., and G. Chong, Late Pliocene age for the Atacama Desert: Implications for the desertification of western South America, *Geology.*, *30*, 43–46, 2002.

Hartley, A. J., and E. J. Jolley, Tectonic implications of Late Cenozoic sedimentation from the Coastal Cordillera of northern Chile (22–24°S), *J. Geol. Soc. London*, *152*, 51–63, 1995.

Hartley, A. J., P. Turner, D. C. Rex, and S. Flint, Palaeomagnetic, geochronological and geological constraints on the tectonic evolution of the Mejillones Peninsula, northern Chile, *Geol. J.*, *27*, 59–74, 1992.

Hartley, A. J., G. May, G. Chong, P. Turner, S. J. Kape, and E. J. Jolley, Development of a continental forearc: A Cenozoic example from the central Andes, northern Chile, *Geology*, *4*, 331–334, 2000.

Hayes, D. E., A geophysical investigation of the Peru-Chile Trench, *Geology*, *4*, 309–351, 1966.

Hilde, T. W. C., Sediment subduction vs. accretion around the Pacific, *Tectonophysics*, *99*, 381–397, 1983.

Hinz, K., et al., Geowissenschaftliche Untersuchungen off- und onshore Zentralanden an der aktiven sudostpazifischen Subduktionszone - CINCA, SONNE-Fahrt SO-104/1, 22.07.-24.08.1995, internal report, Archive 113.998, Bundesanst. für Geowis. und Rohstoffe, Hannover, Germany, 1995.

Hinz, K., et al., Crustal investigations off- and onshore Nazca/central Andes, *Rep. BGR 117.613*, 217 pp., Bundesanst. für Geowis. und Rohstoffe, Hannover, Germany, 1998.

Hojka, A. M., C. A. Zelt, and E. R. Flueh, 3-D seismic refraction tomography of ocean bottom hydrophone data recorded offshore Valparaíso, Chile, *Zentrabl. Geol. Paläontol., Teil I*, *7/8*, 679–693, 2000.

Husen, S., and E. Kissling, Postseismic fluid flow after the large subduction earthquake of Antofagasta, Chile, *Geology*, *29*, 847–850, 2001.

Husen, S., E. Kissling, and E. R. Flueh, Local earthquake tomography of shallow subduction in north Chile: A combined onshore and offshore study, *J. Geophys. Res.*, *105*, 28,183–28,198, 2000.

Jarrard, R. D., Relations among subduction parameters, *Rev. Geophys.*, *24*(2), 217–284, 1986.

Kimura, G., E. Silver, P. Blum, and Leg 170 Scientific Party, *Proceedings of the Ocean Drilling Program*, *Initial Reports*, vol. 170, Ocean Drill. Program, College Station, Tex., 1997.

Koesters, M., H.-J. Götze, S. Schmidt, J. Fritsch, and M. Araneda, Gravity field of a continent-ocean transition mapped from land, air, and sea, *Eos Trans. AGU*, *78*, 13–16, 1997.

Kudrass, H. R., et al., Crustal investigations off- and onshore Nazca/central Andes, CINCA, Sonne-Cruise 104, Leg 3, 16.09.-15.10.1995, internal report, Archive 114.181, 148 pp., Bundesanst. für Geowis. und Rohstoffe, Hannover, Germany, 1995.

Kudrass, H. R., U. von Rad, H. Seyfied, H. Andruleit, K. Hinz, and C. Reichert, Age and facies of sediments of the northern Chilean continental slope-Evidence for intense vertical movements, in *Crustal Investigations Off- and Onshore Nazca/CINCA*), coordinated by K. Hinz and members of the CINCA Study Group, *Rep. BGR 117.613*, pp. 170–196, Bundesanst. für Geowis. und Rohstoffe, Hannover, Germany, 1998.

Kulm, L. D., W. J. Schweller, and A. Masias, A preliminary analysis of the subduction process along the Andean continental margin near 6° to 45°S, in *Island Arcs, Deep-Sea Trenches, and Back-arc Basins*, *Maurice Ewing Ser.*, vol. 1, edited by M. Talwani and W. C. Pitman III, pp. 285–301, AGU, Washington, D. C., 1977.

Lallemand, S., P. Schnurle, and J. Malavieille, Coulomb theory applied to accretionary and nonaccretionary wedges: Possible causes for tectonic erosion and/or frontal accretion, *J. Geophys. Res.*, *99*, 12,033–12,055, 1994.

Mackay, S., and R. Abma, Depth focusing analysis using wavefront-curvature criterion, *Geophysics*, *58*, 1148–1156, 1993.

Mann, J., P. Hubral, B. Traub, A. Gerst, and H. Meyer, Macro-model independent approximative prestrack time migration, paper presented at EAGE 62nd Conference and Technical Exhibition, Eur. Assoc. for Geophys. Explor., Glasgow, Scotland, 29 May to 2 June 2000.

McCarthy, J., and D. W. Scholl, Mechanisms of subduction accretion along the central Aleutian Trench: Geol, *Soc. Am. Bull.*, *96*, 691–701, 1985.

Miller, H., Das Problem des hypothetischen "Pazifischen Kontinentes" gesehen von der chilenischen Pazifikkuste, *Geol. Rundsch.*, *59*, 927–938, 1970.

Niemeyer, H., G. González, and E. Martinez-De Los Rios, Evolución tectónica cenozoica del margen continental activo de Antofagasta, norte de Chile, *Rev. Geol. Chile*, *23*, 165–186, 1996.

Patzig, R., Lokalbeben-Tomographie der Umgebung von Antofagasta (Nordchile) sowie Betrachtungen der Magnituden-Häufigkeits-Parameter in dieser Region, 219 pp., Berliner Geowis. Abh., Fu-Tu-Tfh, Berlin, 2000.

Patzwald, R., J. Mechie, A. Schulze, and P. Giese, Two-dimensional velocity models of the Nazca plate subduction zone between 19.5°S and 25°S from wide-angle seismic measurements during the CINCA95 project, *J. Geophys. Res.*, *104*, 7293–7317, 1999.

Ranero, C. R., and R. von Huene, Subduction erosion along the Middle America convergent margin, *Nature*, *404*, 748–752, 2000.

Ranero, C. R., R. von Huene, E. Flueh, M. Duarte, D. Baca, and K. McIntosh, A cross-section of the convergent Pacific margin of Nicaragua, *Tectonics*, *19*, 335–357, 2000.

Rötzler, K., R. Naumann, and H.-G. Wilke, Tectonic erosion of terrigeneous rocks in northern Chile (19°S and 24°S), in *Crustal Investigations Off- and Oonshore Nazca/Central Andes* (*CINCA*), coordinated by Karl Hinz, *Rep. BGR 117.613*, A-4, 1–14, Bundesanst. für Geowis. und Rohstoffe, Hannover, Germany, 1998.

Rutland, R. W. R., Andean orogeny and ocean floor spreading, *Nature*, *233*, 252–255, 1971.

Saffer, D. M., E. A. Sliver, A. T. Fisher, H. Tobin, and D. Moran, Inferred pore pressures at the Costa Rica subduction zone: Implications for dewatering processes, *Earth Planet. Sci. Lett.*, *177*, 193–207, 2000.

Scheuber, E., Tektonische Entwicklumg des nordchilenischen aktiven Kontinentalrandes: Der Einfluâ von Plattenkonvergenz und Rheologie, 131 pp., *Geotektonische Forschungen*, *81*, E. Schweizerbart'sche, Stuttgart, Germany, 1994.

Scholl, D. W., M. N. Christensen, R. von Huene, and M. S. Marlow, Peru-Chile trench sediments and sea-floor spreading, *Geol. Soc. Am. Bull.*, *81*, 1339–1360, 1970.

Scholl, D. W., R. von Huene, T. L. Vallier, and D. G. Howell, Sedimentary masses and concepts about tectonic processes at underthrust ocean margins, *Geology*, *8*, 564–568, 1980.

Schreckenberger, B., Magnetic modelling, in *Crustal Investigations Off- and Onshore Nazca/Central Andes* (*CINCA*), coordinated by K. Hinz and members of the CINCA Study Group, *Rep. BGR 117.613*, pp. 147–169, Bundesanst. für Geowis. und Rohstoffe, Hannover, Germany, 1998.

Schweller, W. J., and L. K. Kulm, Extensional rupture of oceanic crust in the Chile Trench, *Mar. Geol.*, *28*, 271–291, 1978.

Seely, D. R., P. R. Vail, and G. G. Walton, Trench slope model, in *The Geology of Continental Margins*, edited by C. A. Burk and C. L. Drake, pp. 249–260, Springer-Verlage, New York, 1974.

Tsuru, T., J.-O. Park, N. Takahashi, S. Kodaira, Y. Kido, Y. Kaneda, and Y. Kono, Tectonic features of the Japan Trench convergent margin off Sanriku, northeastern Japan, revealed by multichannel seismic reflection data, *J. Geophys. Res.*, *105*, 16,403–16,413, 2000.

Uyeda, S., and H. Kanamori, Back-arc opening and the mode of subduction, *J. Geophys. Res.*, *84*, 1049–1061, 1979.

Vannucchi, P., D. W. Scholl, M. Meschede, and K. McDougall-Reid, Tectonic erosion and consequent collapse of the Pacific margin of Costa Rica: Combined implications from ODP Leg 170, seismic offshore data, and regional geology of the Nicoya Peninsula, *Tectonics*, *20*, 649–668, 2001.

von Huene, R., and E. Suess, Ocean Drilling Program Leg 112, Peru continental margin, part 1, Tectonic history, *Geology*, *16*, 934–938, 1988.

von Huene, R., Structure of the Andean convergent margin and some implications for hydrocarbon resources, in *Geology of the Andes and Its Relation to Hydrocarbon and Mineral Resources*, edited by G. Ericksen, M. Pinochet, and J. Reinemund, pp. 119–129, Circum-Pac. Counc. for Energy and Miner. Resour., Houston, Tex., 1989.

von Huene, R., and R. Cullotta, Tectonic erosion at the front of the Japan Trench convergent margin, *Tectonophysics*, *160*, 75–90, 1989.

von Huene, R., and S. Lallemand, Tectonic erosion along convergent margins, *Geol. Soc. Am. Bull.*, *102*, 704–720, 1990.

von Huene, R., and D. W. Scholl, Observations at convergent margins concerning sediment subduction, subduction erosion, and the growth of continental crust, *Rev. Geophys.*, *29*(3), 279–316, 1991.

von Huene, R., D. Klaeschen, B. Cropp, and J. Miller, Tectonic structure across the accretionary and erosional parts of the Japan Trench margin, *J. Geophys. Res.*, *99*, 22,349–22,361, 1994.

von Huene, R., I. A. Pecher, and M.-A. Gutscher, Development of the accretionary prism along Peru and material flux after subduction of Nazca Ridge, *Tectonics*, *15*, 19–33, 1996.

von Huene, R., J. Corvalán, E. R. Flueh, K. Hinz, J. Korstgard, C. R. Ranero, and W. Weinrebe, Tectonic control of the subducting Juan Fernández Ridge on the Andean margin near Valparaiso, Chile, *Tectonics*, *16*, 474–488, 1997.

von Huene, R., W. Weinrebe, and F. Heeren, Subduction erosion along the north Chile margin, *J. Geodynamics*, *27*, 345–358, 1999.

von Huene, R., C. R. Ranero, W. Weinrebe, and K. Hinz, Quaternary convergent margin tectonics of Costa Rica, segmentation of the Cocos Plate, and Central American volcanism, *Tectonics*, *19*, 314–334, 2000.

Watts, P., and S. R. Grilli, Tsunami generation by submarine mass failure, I, Wavemaker modes, *J. Waterw. Port Coastal Ocean Eng*, in press, 2002.

Yañez, G. A., C. R. Ranero, R. von Huene, and J. Diaz, Magnetic anomaly interpretation across the southern central Andes (32°–34°S): The role of the Juan Fernandez Ridge in the late Tertiary evolution of the margin, *J. Geophys. Res.*, *106*, 6325–6345, 2001.

C. R. Ranero and R. von Huene, GEOMAR, Research Center for Marine Geosciences, Christian Albrechts University, Wischhofstr 1–3, D-24148 Kiel, Germany. (rhuene@mindspring.com)

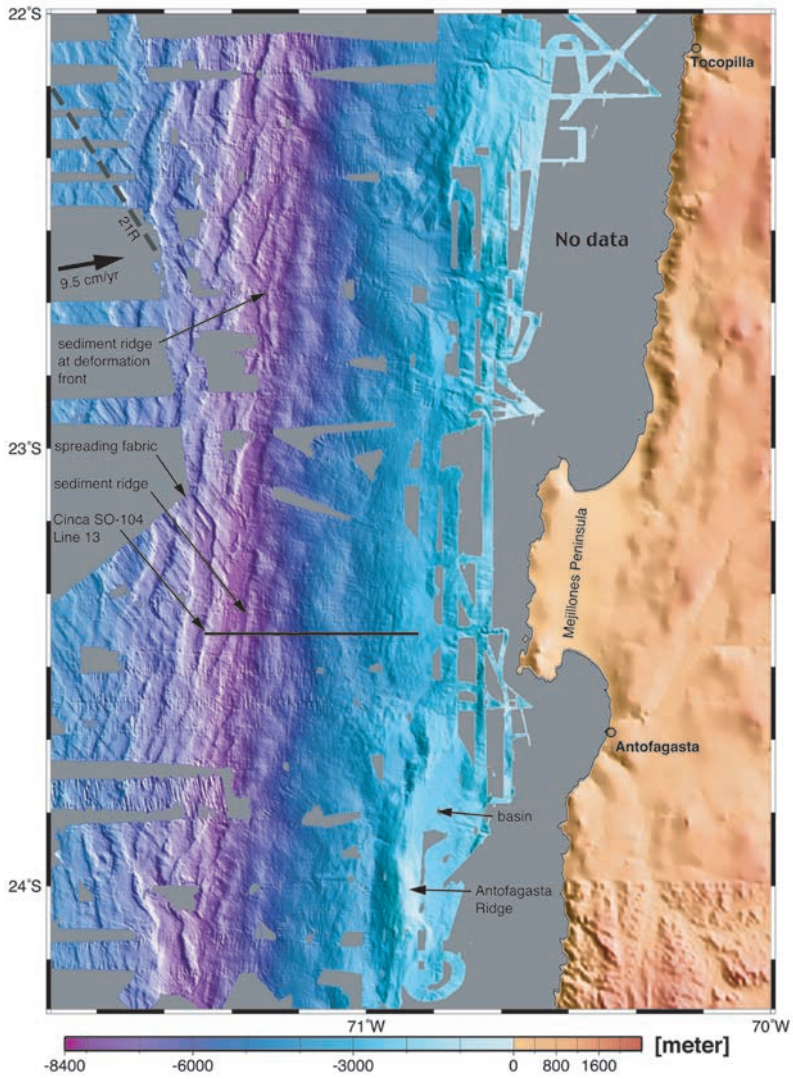

Figure 2. Shaded relief map of swath bathymetry with annotated features. Gray areas indicate no multibeam bathymetric data. CINCA SO104-13 is a multichannel seismic reflection line shown in Figure 5. Sediment ridge refers to slope detritus thrust faulted along the deformation front.